Research Square

Preprints are preliminary reports that have not undergone peer review.
They should not be considered conclusive, used to inform clinical practice,
or referenced by the media as validated information.

Effect of Accelerated Weathering on the Tensile and Flexural Properties of Fused Filament Fabricated ULTEM 9085

Zachary Williams
University of North Florida
Carson Rogers
University of North Florida
Jutima Simsiriwong
University of North Florida
Juan Aceros
jua425@lehigh.edu

Lehigh University

Research Article

Keywords: ULTEM 9085, Fused Filament Fabrication, Mechanical Properties, Ultraviolet Radiation, Accelerated Weathering

Posted Date: November 23rd, 2026

DOI: https://doi.org/10.21203/rs.3.rs-11681222/v1

License: This work is licensed under a Creative Commons Attribution 4.0 International License.
Read Full License

Additional Declarations: No competing interests reported.

Effect of Accelerated Weathering on the Tensile and Flexural Properties of Fused Filament Fabricated ULTEM 9085

Abstract

ULTEM 9085 is a high-performance thermoplastic commonly used in Fused Filament Fabrication (FFF) applications. It is a material well known for its durability in harsh environments; however, its mechanical performance under environmental conditions such as ultraviolet (UV) radiation exposure has not been properly characterized. This study aims to characterize the effects of UV exposure on the tensile and flexural properties of FFF specimens using the ASTM D638 and ASTM D790 standardized test procedures. Specimens were manufactured using a $\pm 45^{\circ}$ raster angle, 100 % infill, 0.254 mm layer height, and two (XY and XZ) layer orientations. Specimens were subjected to five levels of exposure (0 h, 288 h, 576 h, 864 h, and 1152 h) in an accelerated weather tester with four hours of moisture exposure and eight hours of UV exposure in each cycle in accordance with ASTM G154. Mechanical testing results indicate that UV-condensation exposure had a greater affect on the tensile properties of XZ specimens compared to XY. XY specimens saw subtle reductions in yield strength ∼2.7 % and elastic modulus ∼4 % after 1152 h of exposure. XZ specimens, however, saw greater fluctuations in yield strength (+20 %) at 1152 h and elastic modulus (+10.1 %) at 864 h. XZ oriented flexural specimens were superior to XY before exposure, but the weathering process degraded both specimens, where XZ was more impacted and XY displayed greater resilience. XY specimens saw reduction (∼15.4 %, ∼14.3 %, ∼9.7 %) in flexural modulus, flexural strength at 5 % strain, and ultimate strength, where XZ speciemens specimens degraded more dramatically (∼36.7 %, ∼34.5 %, ∼24.4 %). The results show that flexural properties of FFF ULTEM 9085 are more sensitive to weathering than the tensile properties.

Keywords: ULTEM 9085, Fused Filament Fabrication, Mechanical Properties, Ultraviolet Radiation, Accelerated Weathering

1 Introduction

ULTEM 9085 is a high-performance polyetherimide (PEI) and polycarbonate (PC) thermoplastic blend primarily utilized in the fused filament fabrication (FFF) process. It possesses superior thermal and chemical resistance, low toxicity, high fire retardancy, and robust mechanical properties [1]. Its compliance with stringent industry standards

has driven its widespread adoption in the railway and aerospace sectors [2]. While ULTEM 9085 demonstrates reliable performance under standard operating conditions, the mechanical degradation resulting from extended environmental exposure remains largely uncharacterized.

Predicting the viability of ULTEM when subjected to environmental conditions requires understanding the effects of ultraviolet (UV) exposure and excessive moisture. UV exposure is known to induce adverse chemical and physical changes in thermoplastics. Specifically, solar radiation promotes photooxidation, the chemical and physical changes a polymer undergoes as it absorbs radiation, resulting in photodegradation that directly affects the mechanical properties such as stiffness and toughness [3]. Larché [4] found that with increased UV exposure, phenoxy resin, a thermoset, saw an increase in hardness from 100 MPa to approximately 245 MPa. Increased surface hardness is commonly associated with embrittlement and reduced toughness. Tomastik [5] investigated the effects of UV exposure of different additively manufactured (AM) thermoplastics and found consistent results with Larché's study, where materials like ABS (acrylonitrile butadiene styrene) and PETG (polyethylene terephthalate glycol) saw increased hardness with increased exposure.

In addition, exposure to water can lead to chemical degradation in the form of hydrolysis, which breaks down polymer chains, in turn, reducing toughness and decreasing molecular weight. Water absorption can lead to dimensional changes through swelling and lower the glass transition temperature of the polymer, ultimately impairing the overall mechanical performance [6]. The effects of hydrolysis are exacerbated by elevated temperature and relative humidity, which accelerate degradation, cracking, and color fading. González-López et al. [3] examined the hydrolysis rate of PLA (polylactic acid), manufactured via fibers and compression molding, and found that it increased with elevated temperature and relative humidity. Water diffusion in PLA can occur through modes such as micro-gaps between polymer chains, capillary transport into interfaces, and voids introduced by material swelling.

Testing the effects of UV exposure and excessive moisture directly requires exposing specimens to natural conditions over extended periods, an approach often impractical due to time constraints. To reduce the time required for weathering of materials, accelerated weathering (AW) is a commonly employed alternative. AW systems can regulate UV exposure at specimen surfaces, temperature cycling, thermal cycling, and moisture cycles through relative humidity control. By applying elevated, constant temperatures and irradiance, AW accelerates the degradation that natural sunlight would otherwise produce over extensive timescales. A key consideration in this process is determining a light source that closely matches the spectrum of sunlight at Earth's surface. Both Alimi et al. [7] and Real [8] support the use of UVA-340, as UVA comprises over 95 % of the UV experienced at Earth's surface.

Weathering of polymers progresses through two primary mechanisms: chain scission and cross-linking. Chain scission is undesirable as it breaks the entanglement of polymer chains and leads to overall material embrittlement, particularly at the material surface [9]. Scissions and the associated decrease in molecular weight correlate directly with reductions in mechanical properties such as yield strength and elongation at failure [10]. Cross-linking limits molecular mobility and inhibits stress

accommodation under external loading, thereby decreasing resistance to deformation. Batista et al. [11] investigated polyetherimide/carbon fiber composites with various fiber orientations ($0°/+45°/-45°/90°$) subjected to prolonged UV exposure combined with condensation cycles and found that increased exposure resulted in weight loss of the specimens. Governed by photodegradation and plasticization, the specimens in their study underwent three phases of weight changes: an initial decrease through microcracking, an increase through moisture uptake, and a final decrease through photodegradation and polymer leaching [11]. Tocháček [12] further found that elevated exposure temperature during AW reduces the UV dosage required to degrade polypropylene and its copolymers. While temperature alone does not drive photooxidation, their study supports that temperature is responsible for driving its secondary reactions, which is the propagation of oxidation reactions via radical formations [13].

Meides et al. [14] examined the effects of AW on polystyrene (PS). As a commonly utilized polymer, PS offers a useful reference for the degradation pathways and potential failure modes of ULTEM 9085. During the first 400 h of UV exposure, PS showed no notable surface degradation, with the first surface microcracks forming after 800 h. Since the specimens were injection molded, crack formation followed the melted polymer flow direction introduced during processing. Ductility increased up to the 200 h mark, attributable to crosslinking from photooxidation. Beyond 200 h of UV exposure, the specimens embrittled, likely due to polymer chains being too short for effective entanglement [14].

LeBlanc et al. [15] explored the effects of high-pressure saltwater absorption on the mechanical properties of ULTEM 9085. To prepare their specimens, ULTEM was printed on a 3DSystems ProX-800 machine, and tensile testing was conducted in accordance with ASTM D638. Specimens were submerged in saltwater and held in a pressure vessel at 34.5 MPa for 30 and 60 days. It was found that the tensile properties remained relatively constant during aging, with ultimate strength decreasing only marginally from 54.8 MPa to 52.6 MPa. Flexural modulus showed no observable decline, with only a slight 5 % reduction in flexural strength. Their findings support the viability of ULTEM in high salinity environments, though they address a stressor distinct from atmospheric weathering [15].

Wang et al. [16] studied the durability of FFF ULTEM 9085 specimens in marine environments, where they exposed specimens to a large seawater bath, prepared in accordance with ASTM D1141. Specimens were exposed at atmospheric pressure across temperatures of 50 °C, 70 °C, and 90 °C. The tests were conducted over durations of two and four weeks, after which specimens were subjected to mechanical testing. For specimens with layer deposition of $0°/90°$, Wang found that regardless of the temperature in the salt bath, ULTEM 9085 specimens had an increase in stiffness. They also found an increase in the yield strength and ultimate tensile strength. For $\pm 45°$ specimens, however, ultimate tensile strength decreased with increasing exposure time at 70 °C and 90 °C. Irrespective of layering direction, all specimens showed a decrease in strain to failure, consistent with material stiffening under exposure [16].

Despite the works published focusing on marine immersion [15, 16] of FFF ULTEM 9085, there is a lack of investigation on the effects of combined UV and moisture exposure on tensile and flexural properties. Although ULTEM is known for its excellent

chemical resistance and desirable mechanical properties, its response to combined UV and moisture weathering remains largely uncharacterized. Correspondingly, this study aims to establish a baseline for the retention of mechanical properties of ULTEM 9085 specimens produced by FFF subjected to UV and moisture. To simulate atmospheric weathering, specimens were exposed in an accelerated weathering chamber over varying durations. Integrity of specimens will be characterized via mechanical testing, including tensile and flexural tests. Hence, the objectives of this study are (1) quantify retention of tensile and flexural properties with exposure; (2) determine whether the weathering response depends on build orientation; (3) compare the sensitivity of tensile vs flexural loading.

2 Methodology

2.1 Specimen Preparation

ULTEM 9085 specimens in this study were fabricated using a Fortus 450mc industrial 3D printer (Stratasys, Eden Prairie, MN, USA). Two specimen types, including flexural (rectangular) and tensile (dog-bone) specimens, were utilized. Flexural specimens were fabricated in accordance with ASTM D790-17, with nominal dimensions of 12.7 mm × 76 mm × 3.2 mm. Tensile specimens had a gauge section width of 13 mm, depth of 3.2 mm, and a length of 50 mm, following ASTM D638-22 Type I geometry. Both specimen types were fabricated in XY and XZ orientations to facilitate a comparative analysis of anisotropic mechanical behavior. Figure 1 provides a visual representation of these orientations relative to the build platform, illustrating the specific layer-stacking sequences employed during the FFF process.

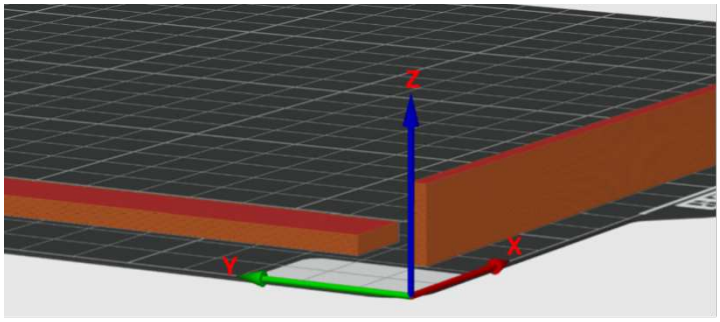


Fig. 1 Simple representation of an XY flexural specimen (left) and an XZ flexural specimen (right) on the build platform.

Recommended print parameters by Stratasys for the Fortus system were utilized, except the infill density and infill pattern. The process parameters are listed in Table 1. Specimens in each orientation were printed independently to maintain consistency within the printer at a given time.

In addition, specimen preparation was conducted in accordance with ASTM F2971-13 (2021). The Fortus printer accommodated two part-material canisters and

Table 1 Process parameters for fabrication of FFF ULTEM 9085 specimens.

Process Parameter	Value
Infill Density	100 %
Raster Infill Pattern	±45°
Nozzle Diameter	T16 (0.4064 mm)
Layer Height	0.25 mm
Number of Contours	1

two support-material canisters, eliminating the necessity of unloading and reloading canisters between prints. The filament was supplied by the manufacturer in a preloaded canister, reducing preprocessing. Since the material could absorb moisture after the canister was opened, specimens were printed immediately after the material was loaded into the Fortus printer. For each print, the slicer automatically positioned the specimens centered on the build platform for optimal printing. Quality was assessed qualitatively; support material was removed fully, no material buildup on the surface, minimal warpage, and no apparent layer adhesion defects.

Standards for flexural and tensile testing recommend a minimum of five specimens per treatment, or dependent variable. 0 h exposure specimens were first printed to establish a baseline, during which material availability permitted five specimens per orientation. The samples were then printed for each orientation to undergo weathering. At the time of XY printing, only enough material was available to produce three specimens for each group. XZ specimens were printed after the XY exposure and testing was conducted; raw material allowed for five specimens per group to be printed. Each orientation was printed independently to maintain consistency within the printer at a given time.

All 24 of the XY weathered specimens were printed simultaneously; however, a limited material supply restricted the number of specimens to three per exposure period. Greater material availability at the time of printing allowed for all five of the XZ specimens per treatment to be produced.

Table 2 Number of FFF ULTEM 9085 specimens tested for each print. orientation and exposure time

	XY		XZ	
Exposure time (h)	Tensile	Flexural	Tensile	Flexural
0	5	5	5	5
288	3	3	5	5
576	3	3	5	5
864	3	3	5	5
1152	3	3	5	5

Per ASTM F3489-23, tensile testing of polymer materials fabricated via material extrusion should default to ASTM D638, with the Type I specimen geometry recommended where possible. Specimens underwent no post-fabrication machining or sanding to avoid introducing defects or surface alterations. Additionally, failure zone classifications for tensile specimens were assigned according to the identifiers outlined in ASTM F3489-23 and are reported in the Results section. ASTM F3489-23 recommends ASTM D790 for flexural testing, from which the modulus of elasticity and flexural strength were determined. Due to the large deformations observed, a traditional yield strength (via 0.2 % offset) could not be readily identified; therefore, a flexural strength at 5 % strain was reported in its place. Ultimate flexural strength was also recorded.

2.2 Accelerated Weathering

Accelerated weathering (AW) was conducted on the tensile and flexural specimens using a Q-Lab QUV/se weathering chamber (Q-Lab, Westlake, OH, USA). The system is equipped with UVA-340+ bulbs operating at a irradiance set point of $0.89\,\mathrm{W\,m^{-2}\,nm^{-1}}$ at 340 nm. Bulb selection was based on ASTM G154-23, using the close spectral match of the UVA-340+ output to natural sunlight. These bulbs produce minimal to no UV output below 295 nm, which is the "cut-on" wavelength for sunlight at the surface.

The exposure cycle consisted of an 8 h UV cycle at a black panel temperature of $(60 \pm 3)\,^{\circ}\mathrm{C}$, followed by a 4 h condensation cycle at $(50 \pm 3)\,^{\circ}\mathrm{C}$ with no UV exposure. The condensation cycle functioned to deposit moisture on specimen surfaces. Four exposure periods were evaluated: 288 h (12 days), 576 h (24 days), 864 h (36 days), and 1152 h (48 days). Exposure periods were influenced by a study published by Afshar and Wood [17], where they FFF specimens for up to 1200 h with groups of 300 h, 600 h, and 1200 h. To simplify the indexing schedule and promote continuous testing, the initial group was reduced by 12 h to have a consistent 12 day group increment. Following this schedule, the final exposure period was 1152 h, just short of the 1200 h practiced by Afshar and Wood [17]. Per ASTM guidelines, the specific exposure period may be determined by mutual agreement between the investigators.

Specimens were rotated at intervals equal to one quarter of the total exposure period to account for irradiance variation across different chamber locations. This rotation schedule followed the manufacturer's recommendations and aligned with ASTM D4329-21 guidelines. Specimens in the 288 h exposure group, for instance, were rotated every 72 h. Interrupting the condensation cycle was avoided by initiating each run with the condensation phase, which ensured that a UV phase concluded precisely at each scheduled rotation interval. This specimen rotation is illustrated in Fig. 2. Tensile specimen panels were indexed one spot to the right, unless they were one of the two rightmost panels. The second from the right, indicated by the red arrow, went to position one, and the rightmost (black) was shifted to position two.

Tensile specimens spanned the full length between specimen panels, extending from screw to screw as shown in Fig. 3a. Only three specimens were able to fit on each specimen panel, exposure groups with five specimens extended to two panels. Flexural specimens being shorter allowed up to six specimens per panel compared to



Fig. 2 Indexing diagram of specimen holder panels in the Q-Lab QUV/se weathering chamber.

only three for the tensile specimens. Flexural test specimens were also rotated 180° at each rotation interval to ensure equivalent UV exposure across all specimens. The rotation of flexural specimens was end-for-end, and the same face was exposed for the entirety of the weathering procedure. For example, specimens in the 288 h group were both indexed and rotated at the 72 h hour mark. The rotation scheme is illustrated in Fig. 3.

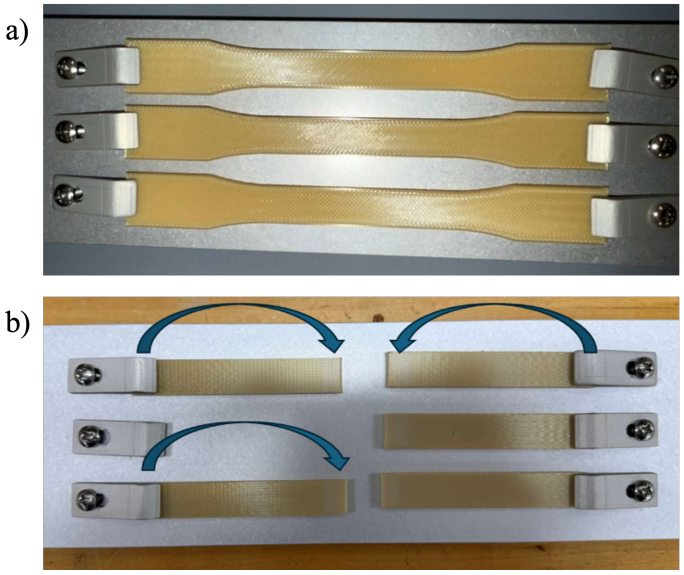


Fig. 3 (a) FFF ULTEM 9085 tensile specimens fixed by screw clamps on the specimen panel and (b) rotation of flexural specimens.

2.3 Tensile and Flexural Testing

Prior to testing, tensile specimens were placed under a vacuum for 24 h to 48 h to remove excess moisture. Following removal from the vacuum, specimen width and

depth were measured. The specimens were prepared and tested in accordance with ASTM D638-22, using serrated grips to minimize slippage during testing and a crosshead swivel mechanism to prevent bending or out-of-plane displacement. Strain was measured using a mechanical extensometer with a 25 mm gauge length (Epsilon Technology Corp Model 3542). Mechanical testing, including both tensile and flexural tests, was performed on a Shimadzu EZ-LX 5 kN tabletop universal mechanical tester. Tensile tests were conducted using a 5 kN load cell at a steady crosshead speed of $5\,\mathrm{mm\,min^{-1}}$ until specimen failure. Data acquisition was collected at 0.01 sec per data point. The following mechanical properties were determined from tensile testing and reported for each specimen: yield strength, ultimate tensile stress, elastic modulus, and strain at break. As no well-defined yield point was identified, a 0.2 % offset was used to determine the yield strength. Ultimate yield strength was taken as the maximum stress value recorded per specimen. Strain at break was taken at the point of fracture.

Flexural specimens were placed under vacuum for 24 h to 48 h prior to testing to remove excess moisture in a similar manner as tensile test samples. Width and depth were recorded following removal from vacuum, as these measurements are required for subsequent calculations, with the exception of the 0 h exposure group. Per ASTM D790-17 Procedure A, the flexural test was conducted in which the crosshead displacement serves as the deflection measurement. Testing was performed in a three-point bending configuration, consisting of two rollers and a cylindrical loading nose as the force applicator. The UV-exposed face of each specimen was placed on the support rollers. Flexural tests were conducted using a 500 N load cell at a steady crosshead speed of $3\,\mathrm{mm\,min^{-1}}$ until specimen failure. Data acquisition was done at a sampling rate of 0.01 sec per data point. The following mechanical properties were determined from flexural testing: flexural stress at 5 % strain, ultimate flexural strength, flexural modulus, and strain at break. The following equations used to calculate flexural strength and strain are given in Eq. 1 and Eq. 2, respectively, as defined in ASTM D790:

$$\sigma_\mathrm{f} = \frac{3PL}{2bd^2} \tag{1}$$

$$\epsilon_\mathrm{f} = \frac{6Dd}{L^2} \tag{2}$$

whereas P is the applied force, D is the maximum deflection of the center of the beam, L is the support span, b is the width of the beam, and d is the depth of the beam. In addition, if the material does not yield or break before or at the 5 % strain limit, the stress at this point is recorded.

3 Results and Discussions

3.1 Tensile Properties

3.1.1 As-Printed Properties and the Effects of Build Orientation

Engineering stress-stain responses were obtained for each test specimen set, evaluating the two printed orientations, XY and XZ. The listed geometries of the specimens, in Appendix A, were recorded after the specimens were subjected to weathering and

placed in vacuum. The tabulated dimensions are consistent among specimens for a given print group and are acceptable compared to the STL/ASTM driven dimensions. Specimens were examined qualitatively for extreme geometric inconsistencies and did not exhibit any abnormalities inhibiting them from analysis. At least three tensile tests were conducted for each set of specimens, and the averaged stress-strain responses were obtained and displayed in Fig. 4. Additionally, tensile properties including the yield strength, ultimate tensile strength, modulus of elasticity, and strain at break, for each set of specimens were calculated.

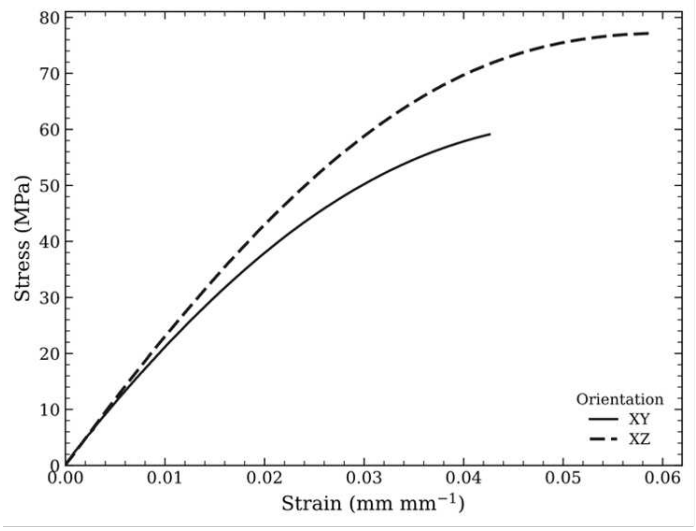


Fig. 4 Engineering stress-strain tensile curve of as-printed FFF ULTEM 9085 specimens fabricated in the XY and XZ directions.

Table 3 includes mechanical properties of ULTEM 9085 found in published studies compared to the results presented in this study. Taking the average value for each mechanical properties, the XY specimens had a percent difference of -11.3 % for yield strength, -0.24 % for UTS, -10 % for elastic modulus, and -11.6 % for strain at break. The XZ specimens saw a -11.7 % change in yield strength, 3.6 % for UTS, -6.59 % for elastic modulus, and -9 % for strain at break. While there is some fluctuation in data, it is not drastically significant and can likely be attributed to specimen preparation. Specimen preparation can vary by raw filament storage and moisture uptake, printer calibration, preparation before testing, and mechanical testing instrumentation. Specimens in this study were generally weaker and resisted less deformation. To improve consistency among studies, thorough preparation and procedures should be documented to reduce any human induced error. XZ specimens showed higher average values for all measured tensile properties. With individual fibers oriented parallel to the loading direction, the XZ specimen displayed the strength of the filament. Layering and raster directions can be seen in Fig. 5, where the loading direction is parallel to the length of the specimens.

Table 3 Tensile properties of as-printed FFF ULTEM 9085 specimens printed in XY and XZ directions compared to published literature.

Source	Yield Strength (MPa)	Ultimate Tensile Strength (MPa)	Elastic Modulus (MPa)	Strain at Break (%)
Experimental				
XY	41.7	61.66	2048	4.7
XZ	48.37	78.58	2298	7
Padovano [18]				
XY	47	65.9	2220	6.6
XZ	54.8	73	2300	8
Vindedze [19]				
XY	-	72.7	2600	-
XZ	-	83.5	2600	-
Zaldivar [20]				
XY	-	46.83	2010	4.03
XZ	-	71.03	2480	7.38

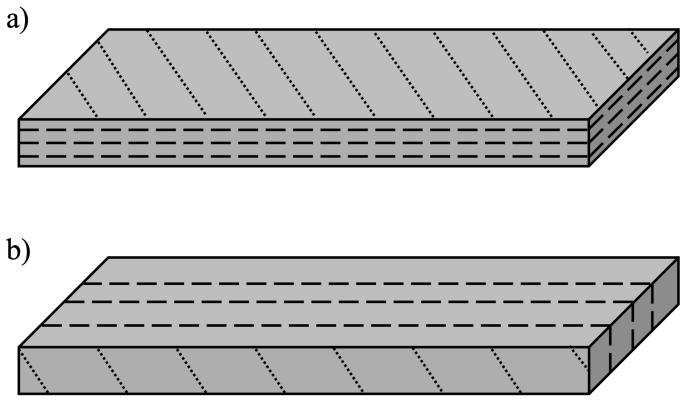


Fig. 5 Simple representation of the contour and infill patterns on (a) XY-oriented specimens and (b) XZ-oriented specimens.

With rasters deposited at a $+45°/-45°$ relative to the loading direction and layering perpendicular to loading, the strength of XY specimens relies on the fusion between layers. Byberg et al. [21] investigated the mechanical properties of FFF ULTEM 9085 and found consistent trends between orientations. With the rasters layered in a $+45°/-45°$ direction and XY/XZ orientations, they found the tensile strength and strain at maximum tensile strength to be superior for XZ specimens. They recorded that XZ specimens had a 7.4 % increase in ultimate tensile strength and strain increased 16.7 %. Padovano et al. [18] also explored the mechanical properties of various print orientations (XY, XZ, and ZX). They found consistent results with Byberg [21] and this study with excellent XZ performance relative to XY, where their specimens had greater yield strength, ultimate strength, and tensile modulus.

The percent difference in mechanical properties of each orientation compared to XZ specimens is recorded in Table 4.

Table 4 Flexural properties of as-printed FFF ULTEM 9085 specimens printed in XY and XZ directions compared to published literature.

Orientation	Yield Strength	Ultimate Tensile Strength	Elastic Modulus
XZ	54.8 MPa	73 MPa	2300 MPa
XY	-14.2 %	-9.7 %	-3.5 %
ZX	-41.6 %	-45.8 %	-7.5 %

Padovano et al. [18] also viewed the specimens under an optical microscope to inspect the voids present at the surface for each orientation. They found the void content of XY specimens to exceed those of the XZ specimens. The voids present in the XY orientation are present at the infill/raster interface as well as the infill area. Conversely, the XZ specimens only saw porosity at the contour/infill interface, with less content than the XY specimens. The lack of filament fusion negatively impacts the overall mechanical performance of the printed parts. Taken together, these results suggest that the improved tensile performance in XZ specimens is associated with a preferential load transfer along the filament direction and reduced porosity. Conversely, XY specimens have higher void content, and load is carried across the interfilament fusion bonds rather than the filament rasters themselves, which degrades the mechanical properties.

3.1.2 Effects of Weathering

Tensile specimen stress-strain curves subjected to weathering are plotted in Fig. 6 with increasing exposure time for both XY and XZ specimens.

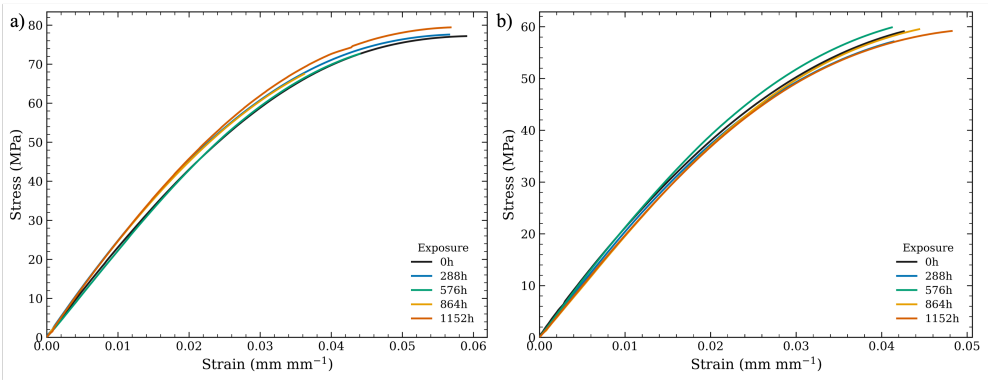


Fig. 6 Averaged stress-strain plots for weathered FFF ULTEM 9085 (a) XZ and (b) XY tensile specimens.

The stress-strain curves show that the orientation is the dominant factor contributing to mechanical properties rather than the influence from weathering. For XY specimens, no significant trends were observed in mechanical properties with increasing exposure. Comparing the 0 h exposure to the 1152 h exposure group, elastic modulus and yield strength both decreased, while the strain at break increased. However, the fluctuation in these properties was mostly insignificant and therefore cannot be directly attributed to weathering, with the exception of the 288 h and 1152 h specimens. Taking the average and standard deviation across all five exposure periods (0 h to 1152 h) for XY specimens, two notable trends are found. First, the elastic modulus, ultimate tensile strength, and strain at break for the 576 h specimen were notably higher than the other exposure groups. Second, the 288 h specimen group had comparatively lower yield an ultimate tensile strength.

For XZ specimens, the elastic modulus, while exhibiting some intrasample variation, remained largely consistent, varying within 5 % from the average of 2340 MPa. This range could be considered sample noise given the small magnitude of deviation. Yield strength varied within 7 % of the average, though the 1152 h specimens displayed a marginally higher strength relative to the other exposure groups, despite not seeing the lowest strain at failure. It would be expected an increased yield strength due to UV exposure would yield a lower material toughness [9]. Strain at break followed a generally linearly decreasing trend with increased exposure, with an exception for the 1152 h group where it increased relative to the other exposure periods. Starting at 7 % strain at break for 0 h of exposure, it decreased to 5.6 % strain at 576 h and partly recovered some toughness at the 1152 h mark with a strain of 6.4 %. Despite this increase, the strain at break for the greatest exposure remain below the 0 h group value.

Changes in the elastic region were small relative to the effect of orientation. Comparing the 1152 h specimens to the 0 h specimens, the average elastic modulus was approximately 2 % lower and the strain at failure decreased by 8 %, but yield strength increased by approximately 20 %. Given that all XZ specimens were printed in the same batch, isolating exposure period as the only variable, the elevated yield strength and reduced strain at failure observed at 1152 h are unexpected results and may indicate microdefects in the polymer surface. Further characterization would be required, such as scanning electron microscopy for porosity or cracks or infrared spectroscopy for changes in functional groups at the surface.

Both orientations were exposed to the weathering conditions outlined, and each orientation exhibited different behavior with increased exposure time. A two-way analysis of variance (ANOVA) with Type II sums of squares was conducted, exploring the effects of orientation, weathering, and their interaction on specimen mechanical properties. Due to the degree of variation in magnitude of strain at failure, the statistical analysis was focused on yield strength and elastic modulus. Degrees of freedom, the F-value, p-value, and partial eta squared are presented in Table 5.

The ANOVA test supports that the yield strength was significantly affected by orientation ($p < 0.001$), and the effect of weathering was orientation dependent, shown by the interaction of orientation:weathering ($p < 0.001$). Although the effect of weathering alone was statistically significant, the interaction indicates this was driven

Table 5 Two-way ANOVA analysis results on tensile properties of weathered FFF ULTEM 9085.

	df	*F*	*p*	η_p^2
Yield Strength				
Orientation	1,29	83.7	<0.001	0.74
Weathering	4,29	10.2	<0.001	0.58
Orientation:Weathering	4,29	6.8	<0.001	0.48
Elastic Modulus				
Orientation	1,29	89.5	<0.001	0.76
Weathering	4,29	3.3	0.025	0.31
Orientation:Weathering	4,29	4.3	0.008	0.37

primarily by XZ specimens rather than a uniform response across orientations. The XY specimens were largely unaffected by weathering, which can be seen in Fig. 7.

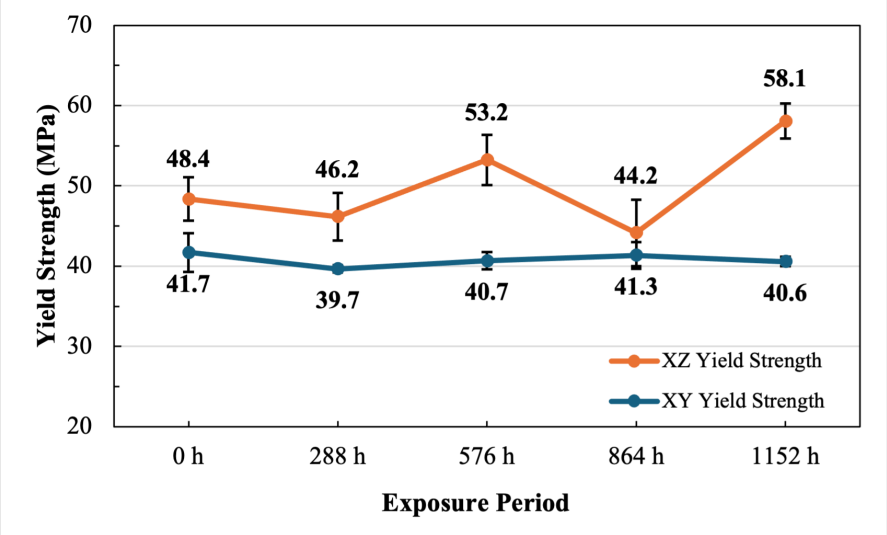


Fig. 7 Mean tensile yield strengths at different exposure periods for FFF ULTEM 9085.

The XY specimens maintained a constant yield strength around 40 MPa, while the XZ specimens had minor fluctuations through intermediate exposures, but ultimately saw a substantial jump of ∼31.5 % from 864 h to 1152 h. This jump contributes to the interaction term between orientation:weathering, highlighting that orientations are affected differently by the effects of weathering. The exposed face of the XZ specimens is a contour side wall, as opposed to XY specimens that expose the top ±45° infill layer. It is possible the surface damage could affect the load carrying filament of XZ specimens more directly.

The statistical analysis of elastic modulus is also recorded in Table 5. Similarly to yield strength, the ANOVA analysis displays that orientation ($p < 0.001$), weathering ($p < 0.025$), and the interaction ($p < 0.008$) were all significant factors. The effects of

orientation were more impactful than weathering, with η_p^2 more than double, which is expected as the XZ specimens mechanically outperformed XY. The interaction here was also notable, as the XZ group reacted differently to weathering than XY. The mean elastic modulus plot for both orientations can be seen in Fig. 8.

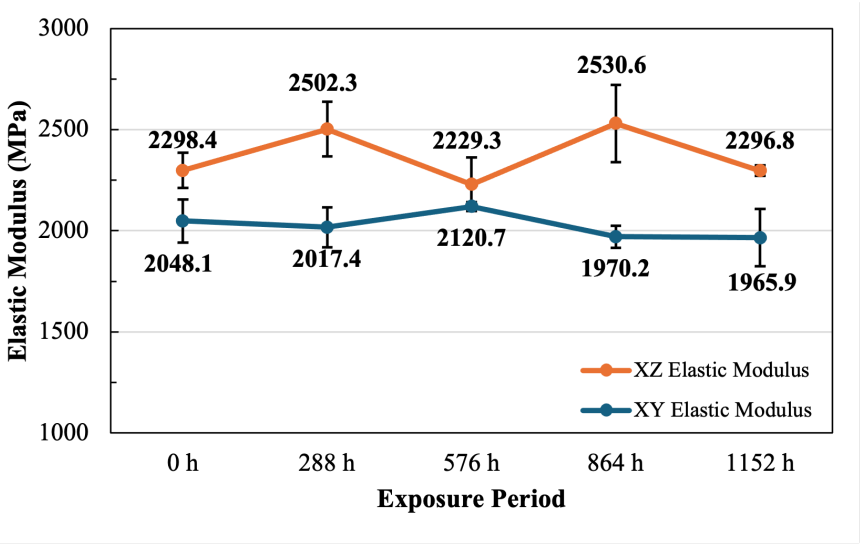


Fig. 8 Mean elastic modulus at different exposure periods for FFF ULTEM 9085.

XY specimens had slight fluctuations around a mean of 2024.4 MPa which can be attributed to noise within the data rather than weathering contribution. At the 288 h and 864 h marks, XZ specimens displayed notable increases in elastic modulus along with decreases in yield strength, seen in Fig. 7, contributing to the interaction term. This combination may reflect a change in deformation behavior, although, the non-monotonic trend across exposure times requires cautious interpretation. Further analysis (via spectroscopy or microscopy) needs to be conducted to understand whether this stiffening was introduced during printing or if it is resultant from weathering. The 0 h, 576 h, and 1152 h are consistent in value for elastic modulus creating difficulty pointing directly towards weathering as the sole contributor.

3.1.3 Failure Behavior

Broken tensile specimens for both orientations can be seen in Fig.9, displaying different failure modes and failure regions. For the XY specimens, the failure region was consistent across all specimens, occurring at the LGT (lateral gauge top) region. The sole exception was specimen 576 h C (boxed in red), which failed at the LGM (lateral gauge middle). Vindedze et al. [19] investigated the mechanical properties of FFF ULTEM 9085, and the failure regions for XY specimens were consistent to those in this study. This specimen also experienced an extensometer issue during testing and was therefore excluded from the tensile results. No failure regions were perfectly

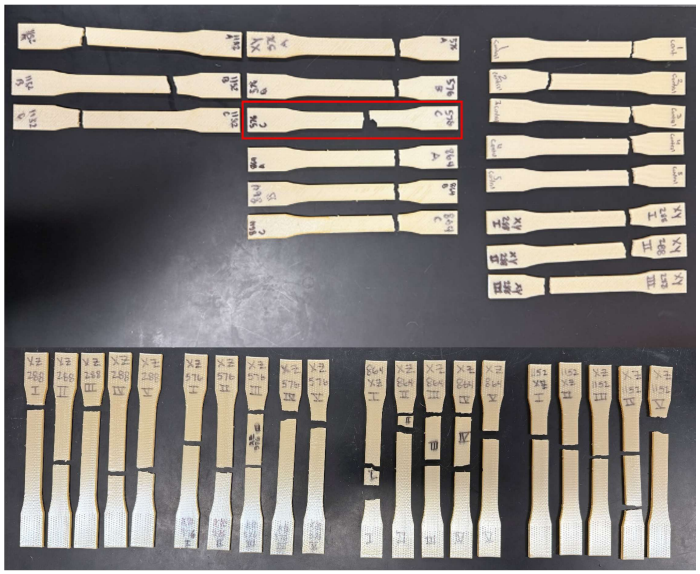


Fig. 9 Fractured (top) XY oriented and (bottom) XZ orientated FFF ULTEM 9085 specimens after post tensile testing.

flat or cleaved, which supports ductile failure experienced by XY specimens. This is also shown in the stress-strain diagrams where the materials clearly yield and do not exhibit brittle failure.

For XZ specimens, when the failure region was consistent within an exposure group, mechanical properties exhibited less variation. There was failure in the LGT and LGM regions, as well as multiple fracture points within the same specimen. The 288 h specimens fractured consistently at the LGT region. The 864 h group, while displaying a mix of ductile and brittle failure modes (characterized by tearing and fine, rigid lines of separation, respectively) were largely consistent in their reported mechanical properties, despite one outlier. The 864 h group had some contribution from potential specimen print defects leading to a larger group variation. Stress-strain plots for each 864 h specimen can be seen in Fig. 10.

There were no known testing discrepancies (extensometer slippage, calibration errors, or improper zeroing of instrument readings), therefore the observed variation is attributed to potential defects within the tensile specimens. The one outlying failed at approximately 67 MPa with a strain of 3.6 % and was excluded from the average and standard deviation calculations.

Elevated variability in strain at failure was also observed for the XZ 576 h and 1152 h exposure groups. The 576 h yielded an average strain at failure of (5.6 ± 0.8) %, while the 1152 h group averaged (6.40 ± 0.75) %. No comparable spread was observed in the other mechanical properties for these groups. The increase in strain at failure from 576 h to 1152 h is counter to the embrittlement behavior typically associated with UV weathering, which is expected to reduce strain with increased exposure [9]. Specimen-level defects, such as insufficient layer fusion or elevated porosity, may also contribute of this behavior. Such defects may introduce inconsistency in mechanical

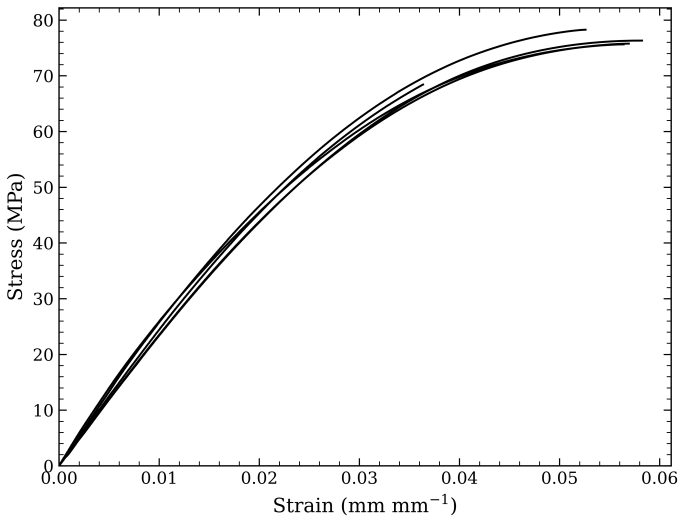


Fig. 10 Stress-strain plot for ULTEM 9085 XZ oriented specimens at 864 h of exposure.

response independent of exposure duration. The 576 h and 1152 h groups exhibited varying fracture locations along the gauge section. UV weathering is known to introduce microcracks at the material surface, and the variability in the density and distribution of these cracks could result in inconsistent crack initiation sites. The variability in initiation sites contributes to the observed scatter in failure location. Xu et al. [22] reported via SEM analysis that weathering induced surface pore formation, which can create stress concentrations and promote premature failure. Surface voids of this nature may be present in the ULTEM specimens, contributing to the observed variability. Additional sources of variability may include inconsistencies in printing between specimens, such as poor layer adhesion or raster misplacement due to print head tip blockage.

3.2 Flexural Properties

3.2.1 As-Printed Properties and the Effect of Build Orientation

Flexural tests were conducted on specimens, and the engineering stress-strain responses were recorded, also exploring XY and XZ orientations. The 0 h of exposure group was tested previously by the research group before exploring the effects of weathering. The dimensions of specimen were not recorded before testing and were faulted to the dimensions in the STL file, not considering the effects of printing (warpage, expansion, or contraction). Specimens, however, did not display any visual defects that would impair test results. At least three specimens per orientation were subjected to the three-point bending test, and the averaged response was determined and displayed in Fig. 11. For each specimen the flexural stress at 5 % strain, max flexural strain, flexural modulus, and strain at break were derived.

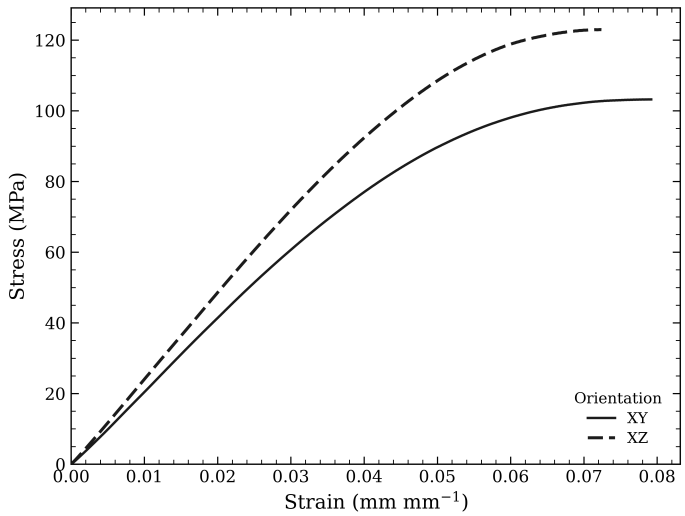


Fig. 11 Averaged stress-strain curves for nonweathered flexural XY and XZ FFF ULTEM 9085 specimens.

Table 6 Flexural properties of as-printed FFF ULTEM 9085 specimens compared with published literature values.

Source	Flexural stress at 5 % strain (MPa)	Flexural strength (MPa)	Flexural modulus (MPa)	Strain at break (%)
Experimental				
XY	91.07	103.25	2059	10.56
XZ	110.29	123.01	2440	10.33
Padovano [18]				
XY	–	109.72	2314	DNF
XZ	–	117.98	2428	DNF
Byberg [21]				
XY	–	102.3	–	–
XZ	–	115.4	–	–

"DNF" = did not fracture; "–" = not reported.

Table 6 displays the flexural properties of ULTEM 9085 found in this study compared to available literature. The flexural properties of ULTEM 9085 are not well documented in published literature, or limited properties are reported for specimens. The data presented in this study is consistent with published literature, where the XZ orientation is better performing than the XY. In all properties except for strain at break, with a 0.23 % decrease, XZ specimens exhibited greater values. Taking the average value of each property from the published literature, XY specimens saw a 2.6 % decrease for ultimate strength and an 11 % decrease in flexural modulus. The

variations in mechanical properties could be a result of differences between experimental approaches. Padovano's [18] preparation and methodology included exposing specimens to a fixed temperature of 87 °C for twelve hours before testing and a slightly increased span length of 51.2 mm compared to 50.8 mm. Additionally, it was not noted in their study which face of the specimen was in tension or compression. Further testing would need to be conducted, but the print bed face could exhibit different properties than the free surface face put in tension in this study.

The flexural modulus found for samples in this study show a 0.5 % increase for XZ specimens and an 11 % decrease for XY. The slight increase for XZ can be attributed to noise, and therefore consistent with published values. However, XY specimens did see a significant drop in material stiffness compared to literature. Padovano [18] printed their specimens with a contour number of three, where this study used a contour number of one. This parameter relates to the number of wall outlines are deposited before the infill for a layer is filled. The additional contours, compared to the contour count of one in this study (Table 1), may contribute to the stiffness of XY specimens, increasing the flexural modulus. Further testing varying the number of contours would be needed to confirm this hypothesis. For the strain at break, Padovano [18] reported that the specimen did not fail, which was defined at a threshold of 9 % strain. For both XY and XZ, strain exceeded 9 % in this study, consistent with published literature.

The performance of XZ versus XY specimens can be attributed to the layering and infill directions. When specimens are subjected to a flexural load, one surface is in tension and the other is in compression. Unlike tensile testing, the load is not evenly distributed within the bulk of the specimen and is a surface-heavy loading. As shown in Fig. 5, the contour versus infill can be seen for each orientation. In a flexural test setup, the XY specimens distribute most of the load against the infill rather than the contour (the wall). Given this distribution, the loading of the infill is split between the fusion strength of adjacent rasters and the filament itself. When placed flat on the rollers, the XZ specimens place the contours parallel to the longitudinal (bending) stress, distributing the force on the surface entirely on the contour. With contours aligned with the bending stress, the resistance of the filament compared to filament plus fusion yields a greater specimen stiffness [18]. Pointed out by Byberg et al. [21], XY specimens exhibit a greater density of incomplete infill/filament fusion at the surface. The incomplete fill and introduced air gaps reduced the available material available for load resistance, influencing a lower strength compared to XZ specimens. Conversely, since the contours compose the XZ surface, the fusion between these comes from direct stacking where sharp angles of infill deposition do not pose concern.

3.2.2 Effect of Weathering

Stress-strain curves for flexural specimens subjected to weathering are plotted in Fig. 12.

Stress-strain curves show that there is noticeable spread in the performance of an orientation as it is increasingly exposed to weathering. Figure 12a represents the weathering XY specimens, which visually separates the outlying group of 288 h of exposure. These specimens represent a transient improvement in flexural behavior,

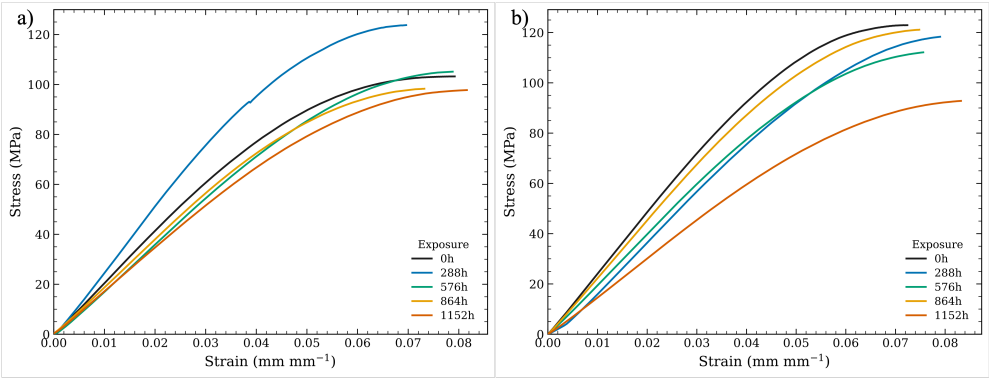


Fig. 12 Averaged stress-strain plot for weathered (a) XY oriented and (b) XZ oriented FFF ULTEM 9085 flexural specimens.

greatly outside the envelope of all other groups. While less tightly bounded stress-strain curves shown in Fig. 12b, XZ specimens did however see a grouping in flexural performance, with an outlying group at 1152 h of exposure. This suggests that the performance was more consistent until the greatest period, where the specimens saw the greatest effect from weathering degradation.

The XZ specimens exhibited a greater fluctuation in performance when subjected to the weathering exposure. Unlike the tensile properties, which saw ∼5 % variation from the mean between exposure groups in the elastic region, the flexural performance varied from the elastic to plastic regime. Relative to the 0 h group, the flexural modulus of XZ specimens saw variation, peaking at a 37 % decrease for 1152h of exposure, and XY specimens with a 28 % increase at 288 h. The significance of this shows the influence of weathering on the elastic properties of ULTEM 9085 varies in tension versus flexion. Unlike tensile properties, the variation in property performance cannot be directly attributed to sample noise, rather the influence of weathering is significant when performing flexural tests. As mentioned, the effect of weathering are isolated to the surface of the specimens, leading to a thin surface layer of degradation. When the weathered tensile specimens are subjected to loading, the applied force is evenly distributed throughout the bulk of the gauge section. The dispersion of force reduces the influence the weathered face has on the specimen behavior. This distribution is not common for flexural specimens, where the exposed face is placed in tension and the unexposed face is under compression. Applying tension to the exposed face exacerbates the degradation caused by weathering, locating the highest stress on this face. Defects such as microcracks present on tensile and flexural specimens would exhibit different stress concentrations, where flexural testing has the greatest stress on the exposed face and tensile testing has uniform stress on all faces.

Generally, the flexural modulus for both orientations saw a decrease as the exposure period increased, XZ specimen dropping ∼37 % from as-printed to 1152 h of exposure and XY specimens ∼15 %. XZ specimens initially had a greater yield and ultimate strength and retained superior strength until the 1152 h mark. XY specimens ended with a ∼9 % greater flexural stress at 5 % strain and a ∼5 % greater ultimate

strength compared to XZ specimens. XZ degraded more severely in each property, while XY specimens exhibited a more balanced resistance to weathering.

To further understand the influence of orientation, weathering exposure, and their interaction, a two-way ANOVA analysis was completed, similar to tensile specimens. The results are listed in Table 7.

Table 7 Two-way ANOVA analysis results on flexural properties of weathered FFF ULTEM 9085.

	df	*F*	*p*	η_p^2
Flexural Modulus				
Orientation	1,28	0.603	0.444	0.021
Weathering	4,28	63.326	<0.001	0.900
Orientation:Weathering	4,28	25.845	<0.001	0.787
Ultimate Strength				
Orientation	1,28	39.004	<0.001	0.582
Weathering	4,28	54.310	<0.001	0.886
Orientation:Weathering	4,28	23.251	<0.001	0.789
Flexural Stress at 5 % Strain				
Orientation	1,28	6.964	0.013	0.199
Weathering	4,28	67.747	<0.001	0.906
Orientation:Weathering	4,28	43.602	<0.001	0.862

The ANOVA results support that flexural modulus had statistically significant influence from weathering and that the effects of exposure had orientation-dependent behavior. While the effect of orientation was not directly significant, it is worth noting that its presence arises in the interaction, thus showing importance at certain exposure periods. However, for ultimate strength, it is seen that orientation, weathering, and the interaction were all statistically significant factors in the flexural properties of specimens. The same trend is seen for the flexural stress at 5 % strain. Within the conditions tested, XY and XZ orientations with five exposure periods, weathering had the largest effects on all three flexural properties. With a η_p^2 of 0.886 and 0.906 for ultimate strength and flexural stress at 5 % strain, weathering was the prominent factor, followed by orientation:weathering interaction (0.787 and 0.862), and orientation (0.021 and 0.582). The strong interaction factor indicates that the effect of weathering depends on build orientation.

The ANOVA analysis alone supports that these factors influence behavior but does not provide insight into which specific pairs differ. A Tukey test was performed on the mechanical properties to help identify which groups were affected by the different factors. The Tukey results are listed in Table 8.

In Table 8, superscript letters compare weathering times within each orientation and property, where groups sharing the same letter are not statistically different (Tukey HSD, $\alpha = 0.05$). Sample sizes were $n = 3$ for all XY groups and the XZ 0 h group, and $n = 5$ for weathered XZ groups; this variation reflects material availability at the time of testing. Groups with an asterisk denote that an orientation has a significantly higher property value a specific weathering time, without an asterisk, they are not significantly different. Given the limited sample sizes of XY specimens and the

Table 8 Flexural properties (mean ± standard deviation) of XY oriented and XZ oriented FFF ULTEM 9085 specimens at each exposure duration.

Property	Orientation	Control	288 h	576 h	864 h	1152 h
Flexural chord modulus (MPa)	XY	2059 ± 64^{b}	$2642 \pm 159^{a*}$	1880 ± 59^{bc}	1925 ± 28^{bc}	1742 ± 65^{c}
	XZ	$2440 \pm 19^{a*}$	2150 ± 158^{bc}	2024 ± 132^{c}	$2286 \pm 87^{ab*}$	1546 ± 13^{d}
Ultimate strength (MPa)	XY	103.3 ± 1.2^{b}	124.1 ± 3.6^{a}	105.2 ± 3.1^{b}	98.4 ± 1.7^{b}	97.9 ± 1.7^{b}
	XZ	$123.0 \pm 0.7^{a*}$	118.9 ± 6.0^{ab}	112.9 ± 5.9^{b}	$121.3 \pm 2.6^{a*}$	93.2 ± 0.9^{c}
5 % offset yield strength (MPa)	XY	91.1 ± 2.9^{b}	$113.9 \pm 5.4^{a*}$	84.9 ± 2.9^{bc}	81.8 ± 1.7^{bc}	78.0 ± 2.8^{c}
	XZ	$110.3 \pm 2.2^{a*}$	91.9 ± 4.5^{b}	92.4 ± 5.8^{b}	$102.9 \pm 3.4^{a*}$	71.7 ± 0.5^{c}

XZ 0 h group, non-significant results should not be concluded as support properties are unaffected by weathering, rather, the results for these groups are inconclusive.

The Tukey analysis shows that as-printed XZ specimens are superior to XY specimens, with XZ significantly higher in all three properties at 0 h. After 288 h of exposure, this relationship reversed for stiffness and yield strength. XY specimens increased drastically relative to the 0 h group in all three properties, approximately 28 % in flexural modulus, 20 % in ultimate strength, and 25 % in the flexural stress at 5 % strain. These values were significantly greater than XZ in flexural modulus and yield strength. Ultimate strength did not differ greatly at 288 h. Over the same period, XZ specimens retained their ultimate strength but showed significant reductions in flexural modulus and yield strength relative to the 0 h group, 12 % and 17 %, respectively.

At 576 h, the XY increase was no longer apparent. XY specimens returned to values statistically equivalent to their 0 h group in all three properties, while XZ specimens remain significantly below their 0 h group. The two orientations were not significantly different in any property at this exposure period. At 864 h, though, XZ specimens recovered to values statistically equivalent to their 0 h group in all three properties, thus, a significant increase from 576 h. XY specimens remained relatively consistent with their 0 h group, and XZ was again substantially higher than XY in all three properties. This change in behavior at 864 h reproduced the orientation relationship observed in the as-printed condition.

At 1152 h, no significant difference between orientations was present in any property, indicating the orientation effect observed at shorter exposures was lost. Both orientations showed significant reductions relative to their 0 h groups in flexural modulus and yield strength, while XY ultimate strength remained statistically equivalent to its 0 h group. XZ specimens showed larger relative reductions, approximately 37 % in flexural modulus, 24 % in ultimate strength, and 35 % in flexural stress at 5 % strain, compared to the 15 %, 5 %, and 14 % of XY. As XZ began with higher property values, the larger reductions brought the two orientations to statistically equivalent properties.

Changes were consistent across all three properties and may be due to a physical attribute driving behavior. There was an increase in XY specimens at 288 h, the

recovery of XZ specimens between 576 h and 864 h, and the overall reduction of properties in XZ at 1152 h, with the lowest values in each property. The 288 h specimens saw an increase in all three properties, which is unlikely to be an artifact of a single property measurement. It is possible that stiffening or some strengthening mechanism was present at this exposure period that impacted XY specimens more than XZ. In all three cases, further characterization must be explored to understand the root cause. It is possible that weathering could have formed new molecules at the surface as a byproduct of weathering that stiffened the material via cross-linking. Scanning electron microscopy or optical microscopy imaging could also be done to identify any surface defects contributing to poor XZ performance.

Within the exposures tested, the preferred orientation depends on the intended exposure. In the as-printed condition, XZ is the better performing orientation. Between 288 h and 864 h of exposure, XY properties were statistically equivalen or greater than their as-printed values, where the XZ properties fluctuated. XZ specimens fell below the as-printed values at the 288 h mark, for flexural modulus and yield strength, and at the 576 h mark for all three properties before recovering at 864 h. XY was able to maintain greater stability in performance through intermediate exposure, although its 288 h increase was transient and need explored further. At 1152 h, the orientations were statistically equivalent, and neither retained an advantage at the longest exposure period. The commonality in specimens to experience degradation at the 1152 h mark could be contributed to adverse effects of weathering, such as surface degradation, either microcracks, pitting, or delamination [11].

4 Conclusion

This study investigated the effect of accelerated UV-condensation weathering on the mechanical properties of FFF ULTEM 9085. Specimens were fabricated in XY and XZ orientations with 100 % infill, layer height of 0.254 mm, a T16 tip, and an infill pattern of $\pm 45°$, which were then subjected to four exposure periods of 288 h, 576 h, 864 h, and 1152 h. Following weathering, the tensile and flexural mechanical behavior properties of the specimens were obtained, and the following conclusions can be drawn from the results:

1. Build orientation governed the as-printed tensile and flexural properties of FFF ULTEM 9085 specimens. Before weathering, specimens fabricated in XZ direction outperformed those fabricated in XY specimens in both uniaxial tensile and three-point bending loadings, with approximately 16 % higher yield strength, 27 % higher ultimate tensile strength, and 12 % higher elastic modulus in tension, and approximately 19 % higher flexural modulus and ultimate flexural strength in bending. This advantage arises because the filaments and contours in XZ specimens are aligned with the principal stress, whereas XY specimens rely on interfilament fusion between $\pm 45°$ rasters.
2. Despite their lower initial performance, FFF ULTEM 9085 specimens fabricated in XY direction retained their flexural and tensile properties more consistently than those fabricated in XZ specimens across the exposure periods. Since the build orientation that performs best in the as-printed condition may not provide the

best performance after prolonged outdoor exposure, build orientation should be selected based on the anticipated service environment.

3. Flexural properties of FFF ULTEM 9085 specimens were observed to be more considerably sensitive to weathering than tensile specimens. UV-condensation weathering produced a thin degraded layer on the exposed surface, influencing greater sensitivity of flexural properties to weathering. Under uniaxial tension, stress is uniformly distributed across the gauge cross-section; therefore, the degraded layer carries only a small fraction of the applied load. In flexure, however, the exposed surface is subjected to the maximum tensile stress, making the degraded layer more influential on mechanical performance. This effect was most pronounced in specimens fabricated in XZ directions, where ultimate tensile strength slightly increased ($\sim$1.3 %), while flexural strength substantially decreased ($\sim$24.2 %).

Some limitations in this study should be noted. Due to a limited sample size per group, especially in the XY orientation, statistical power was limited. Therefore, non-significant differences in these groups are inconclusive rather than evidence of no effect. In addition, no chemical or microstructural characterization was performed in this study; therefore, the proposed degradation mechanisms remain hypothetical. Future work should include a larger sample size and longer total exposure durations. Surface characterization using Fourier transform infrared spectroscopy and scanning electron microscopy should also be performed to examine and validate the degradation mechanisms of weathered FFF ULTEM 9085 specimens.

Statements and Declarations

Declaration of competing interest. The authors declare that they have no known competing financial interests or personal relationships that could have appeared to influence the work reported in this paper.

Data availability. Data will be made available upon request.

Appendix A Specimen Dimensions

Table A1 Measured dimensions of flexural and tensile specimens at each exposure time for XY oriented FFF ULTEM 9085.

		Flexural specimens		Tensile specimens	
Exposure time (h)	Sample	Width (mm)	Thickness (mm)	Width (mm)	Thickness (mm)
288	a	12.92	3.52	13.17	3.65
	b	12.82	3.49	13.15	3.60
	c	12.89	3.48	13.10	3.52
576	a	12.79	3.49	13.10	3.51
	b	12.76	3.49	13.13	3.52
	c	12.80	3.47	13.11	3.49
864	a	12.80	3.54	13.14	3.51
	b	12.80	3.55	13.20	3.56
	c	12.75	3.49	13.26	3.59
1152	a	12.92	3.70	13.20	3.51
	b	12.90	3.50	13.15	3.50
	c	12.94	3.52	13.15	3.51

Table A2 Measured dimensions of flexural and tensile specimens at each exposure time for XZ oriented FFF ULTEM 9085.

		Flexural specimens		Tensile specimens	
Exposure time (h)	Sample	Width (mm)	Thickness (mm)	Width (mm)	Thickness (mm)
288	a	13.02	3.23	13.71	3.33
	b	13.00	3.26	13.71	3.43
	c	13.01	3.26	13.74	3.41
	d	13.02	3.38	13.71	3.35
	e	13.00	3.41	13.70	3.33
576	a	13.02	3.52	13.65	3.41
	b	13.02	3.37	13.66	3.35
	c	12.98	3.32	13.66	3.39
	d	13.01	3.46	13.68	3.49
	e	13.03	3.43	13.67	3.36
864	a	13.01	3.23	13.61	3.36
	b	13.00	3.23	13.69	3.31
	c	13.01	3.32	13.61	3.43
	d	13.00	3.29	13.70	3.40
	e	13.00	3.29	13.72	3.39
1152	a	12.92	3.75	13.65	3.30
	b	12.92	3.75	13.57	3.43
	c	12.92	3.76	13.57	3.36
	d	12.92	3.76	13.55	3.33
	e	12.88	3.75	13.59	3.30

References

[1] Stratasys (2026) Ultem 9085 production-grade thermoplastic for fortus 3d printers. URL https://www.stratasys.com/en/materials/materials-catalog/fdm-materials/ultem-9085/, accessed 02 November 2026

[2] Boado-Cuartero B, Pérez-Álvarez J, Roibás-Millán E (2024) Material characterization of high-performance polymers for additive manufacturing (am) in aerospace mechanical design. Aerospace 11(9). https://doi.org/10.3390/aerospace11090748, URL https://www.mdpi.com/2226-4310/11/9/748

[3] González-López ME, Martín del Campo AS, Robledo-Ortíz JR, et al (2020) Accelerated weathering of poly(lactic acid) and its biocomposites: A review. Polymer Degradation and Stability 179:109290. https://doi.org/https://doi.org/10.1016/j.polymdegradstab.2020.109290, URL https://www.sciencedirect.com/science/article/pii/S0141391020302226

[4] Larché JF, Bussière PO, Thérias S, et al (2012) Photooxidation of polymers: Relating material properties to chemical changes. Polymer Degradation and Stability 97(1):25–34. https://doi.org/https://doi.org/10.1016/j.polymdegradstab.2011.10.020, URL https://www.sciencedirect.com/science/article/pii/S0141391011003612

[5] Tomastik J, Siskova K, Vaclavek L, et al (2026) Only skin deep? depth-resolved photo-oxidation of 3d printed polymers pla, abs, petg, hips and pc after 322 days of continuous uv exposure. Materials Today Communications 57:116436. https://doi.org/https://doi.org/10.1016/j.mtcomm.2026.116436, URL https://www.sciencedirect.com/science/article/pii/S2352492826018258

[6] Maxwell AS, Broughton WR, Dean GD, et al (2005) Review of accelerated ageing methods and lifetime prediction techniques for polymeric materials. NPL Report DEPC MPR 016, National Physical Laboratory, Teddington, UK

[7] Alimi OS, Claveau-Mallet D, Kurusu RS, et al (2022) Weathering pathways and protocols for environmentally relevant microplastics and nanoplastics: What are we missing? Journal of Hazardous Materials 423:126955. https://doi.org/https://doi.org/10.1016/j.jhazmat.2021.126955, URL https://www.sciencedirect.com/science/article/pii/S0304389421019233

[8] Real LEP (2023) Artificial Accelerated Weathering, Springer Nature Switzerland, Cham, pp 53–83. https://doi.org/10.1007/978-3-031-33285-2_4, URL https://doi.org/10.1007/978-3-031-33285-2_4

[9] Puttonen T, Salmi M, Partanen J (2021) Mechanical properties and fracture characterization of additive manufacturing polyamide 12 after accelerated weathering. Polymer Testing 104:107376. https://doi.org/https://doi.org/10.1016/j.polymertesting.2021.107376, URL https://www.sciencedirect.

com/science/article/pii/S0142941821003214

[10] Cho C, Nam SL, de la Mata AP, et al (2022) Investigation of the accelerated thermal aging behavior of polyetherimide and lifetime prediction at elevated temperature. Journal of Applied Polymer Science 139(15):51955. https://doi.org/https://doi.org/10.1002/app.51955, URL https://onlinelibrary.wiley.com/doi/abs/10.1002/app.51955, https://onlinelibrary.wiley.com/doi/pdf/10.1002/app.51955

[11] Batista NL, Iha K, Botelho EC (2013) Evaluation of weather influence on mechanical and viscoelastic properties of polyetherimide/carbon fiber composites. Journal of Reinforced Plastics and Composites 32(12):863–874. https://doi.org/10.1177/0731684413482994, URL https://doi.org/10.1177/0731684413482994, https://doi.org/10.1177/0731684413482994

[12] Tocháček J, Vrátníčková Z (2014) Polymer life-time prediction: The role of temperature in uv accelerated ageing of polypropylene and its copolymers. Polymer Testing 36:82–87. https://doi.org/https://doi.org/10.1016/j.polymertesting.2014.03.019, URL https://www.sciencedirect.com/science/article/pii/S0142941814000774

[13] Yousif E, Haddad R (2013) Photodegradation and photostabilization of polymers, especially polystyrene: review. SpringerPlus 2(1):398. https://doi.org/10.1186/2193-1801-2-398, URL https://doi.org/10.1186/2193-1801-2-398

[14] Meides N, Menzel T, Poetzschner B, et al (2021) Reconstructing the environmental degradation of polystyrene by accelerated weathering. Environmental Science & Technology 55(12):7930–7938. https://doi.org/10.1021/acs.est.0c07718, URL https://doi.org/10.1021/acs.est.0c07718, https://pubs.acs.org/esthag/article-pdf/55/12/7930/3698906/es0c07718.pdf

[15] LeBlanc J, Shattuck L, Warner E, et al (2023) Effect of high pressure salt water absorption on the mechanical characteristics of additively manufactured polymers. International Journal of Lightweight Materials and Manufacture 6(3):379–391. https://doi.org/https://doi.org/10.1016/j.ijlmm.2022.12.001, URL https://www.sciencedirect.com/science/article/pii/S2588840422000841

[16] Wang XJ, Travis C, Sorna MT, et al (2024) Durability of ultem 9085 in marine environments: A consideration in fused filament fabrication of structural components. Polymers 16(3). https://doi.org/10.3390/polym16030350, URL https://www.mdpi.com/2073-4360/16/3/350

[17] Afshar A, Wood R (2020) Development of weather-resistant 3d printed structures by multi-material additive manufacturing. Journal of Composites Science 4(3). https://doi.org/10.3390/jcs4030094, URL https://www.mdpi.com/2504-477X/4/3/94

[18] Padovano E, Galfione M, Concialdi P, et al (2020) Mechanical and thermal behavior of ultem® 9085 fabricated by fused-deposition modeling. Applied Sciences 10(9). https://doi.org/10.3390/app10093170, URL https://www.mdpi.com/2076-3417/10/9/3170

[19] Vīndedze E, Glaskova-Kuzmina T, Dejus D, et al (2025) Effects of printing orientation on the tensile, thermophysical, smoke density, and toxicity properties of ultem® 9085. Polymers 17(2). https://doi.org/10.3390/polym17020145, URL https://www.mdpi.com/2073-4360/17/2/145

[20] Zaldivar R, Witkin D, McLouth T, et al (2017) Influence of processing and orientation print effects on the mechanical and thermal behavior of 3d-printed ultem® 9085 material. Additive Manufacturing 13:71–80. https://doi.org/https://doi.org/10.1016/j.addma.2016.11.007, URL https://www.sciencedirect.com/science/article/pii/S2214860416301609

[21] Byberg KI, Gebisa AW, Lemu HG (2018) Mechanical properties of ultem 9085 material processed by fused deposition modeling. Polymer Testing 72:335–347. https://doi.org/https://doi.org/10.1016/j.polymertesting.2018.10.040, URL https://www.sciencedirect.com/science/article/pii/S0142941818312923

[22] Xu B, van den Hurk B, Liu T, et al (2024) Effect of uv-water weathering on the mechanical properties of flax-fiber-reinforced polymer composites. Polymer Composites 45(5):4266–4280. https://doi.org/https://doi.org/10.1002/pc.28057, URL https://4spepublications.onlinelibrary.wiley.com/doi/abs/10.1002/pc.28057, https://4spepublications.onlinelibrary.wiley.com/doi/pdf/10.1002/pc.28057